



# Improving sub-canopy snow depth mapping with unmanned aerial vehicles: lidar versus structure-from-motion techniques

Phillip Harder<sup>1</sup>, John W. Pomeroy<sup>1</sup>, and Warren D. Helgason<sup>1,2</sup>

<sup>1</sup>Centre for Hydrology, University of Saskatchewan, Saskatoon, Saskatchewan, Canada

<sup>2</sup>Department of Civil, Geological, and Environmental Engineering, University of Saskatchewan, Saskatoon, Saskatchewan, Canada

**Correspondence:** Phillip Harder (phillip.harder@usask.ca)

Received: 23 November 2019 – Discussion started: 16 December 2019

Revised: 29 April 2020 – Accepted: 5 May 2020 – Published: 15 June 2020

**Abstract.** Vegetation has a tremendous influence on snow processes and snowpack dynamics, yet remote sensing techniques to resolve the spatial variability of sub-canopy snow depth are not always available and are difficult from space-based platforms. Unmanned aerial vehicles (UAVs) have had recent widespread application to capture high-resolution information on snow processes and are herein applied to the sub-canopy snow depth challenge. Previous demonstrations of snow depth mapping with UAV structure from motion (SfM) and airborne lidar have focussed on non-vegetated surfaces or reported large errors in the presence of vegetation. In contrast, UAV-lidar systems have high-density point clouds and measure returns from a wide range of scan angles, increasing the likelihood of successfully sensing the sub-canopy snow depth. The effectiveness of UAV lidar and UAV SfM in mapping snow depth in both open and forested terrain was tested in a 2019 field campaign at the Canadian Rockies Hydrological Observatory, Alberta, and at Canadian prairie sites near Saskatoon, Saskatchewan, Canada. Only UAV lidar could successfully measure the sub-canopy snow surface with reliable sub-canopy point coverage and consistent error metrics (root mean square error (RMSE)  $<0.17$  m and bias  $-0.03$  to  $-0.13$  m). Relative to UAV lidar, UAV SfM did not consistently sense the sub-canopy snow surface, the interpolation needed to account for point cloud gaps introduced interpolation artefacts, and error metrics demonstrated relatively large variability (RMSE  $<0.33$  m and bias  $0.08$  to  $-0.14$  m). With the demonstration of sub-canopy snow depth mapping capabilities, a number of early applications are presented to showcase the ability of UAV lidar to effectively

quantify the many multiscale snow processes defining snowpack dynamics in mountain and prairie environments.

## 1 Introduction

Snow accumulation and melt are critical parts of the hydrological cycle in cold regions (King et al., 2008). To understand these processes, there needs to be robust and accurate observation methodologies to measure the depth and density of a snowpack and its change across all aspects of the landscape. Unfortunately, satellite remote sensing methods struggle to quantify the spatial distribution of snow at a high enough resolution and accuracy to account for the fine-scale interactions between snow and vegetation (Nolin, 2010). Remote sensing conceptually promises the capability to gather this type of data at the spatial scales and extents needed, but the main challenge for snow observations across a heterogeneous landscape is that exposed vegetation and forests obscure the underlying snow surface (Bhardwaj et al., 2016; Nolin, 2010; Tinkham et al., 2014). This paper seeks to illuminate some of the challenges posed to unmanned aerial vehicle (UAV) based remote sensing of snow depth observations and how UAV lidar represents a promising opportunity to overcome this limitation at the small catchment scale ( $< 5$  km<sup>2</sup>).

Capturing the spatial distribution of snowpacks and snow cover at a particular instance provides information about the integrated accumulation and ablation processes up to that point in time. Accurate quantification of snow accumulation and ablation is needed to improve the understanding of snow

hydrology, test processes, examine the spatial scaling of process interactions (Clark et al., 2011; Deems et al., 2006; Trujillo et al., 2007), and to initialise and/or validate model predictions (Hedrick et al., 2018). Snow depth, the focus of this paper, is not the variable of ultimate interest for hydrology. Rather, snow water equivalent (SWE) is used for snow hydrology applications (Pomeroy and Gray, 1995). Fully cognisant of this, the focus here is on snow depth, as it is well documented that snow depth varies much more than density (Pomeroy and Gray, 1995; Shook and Gray, 1996; Jonas et al., 2009; López-Moreno et al., 2013); therefore, improving the accuracy of snow depth observations in a drainage basin is critical to improving the estimation of SWE at and within basin scales.

Snow depth and SWE observations are traditionally collected through in situ observations (Goodison et al., 1987; Helms et al., 2008; Kinar and Pomeroy, 2015a; Sturm, 2015). In situ approaches, such as snow surveying, rely on manual sampling of snow depths and densities to get SWE. When conducted along landscape-stratified transects, the landscape-scale SWE can be estimated (Pomeroy and Gray, 1995; Steppuhn and Dyck, 1974). The challenge for snow survey observations is that they are prone to observer bias, are labour-intensive and time-consuming, and are often unable to sample all aspects of a landscape such as avalanche zones (Kinar and Pomeroy, 2015a). Nonetheless, snow surveying is a proven approach to quantify SWE and has been operationalised across many regions. The practice has historical precedence and has created many long-term records which are a valuable data source (Goodison et al., 1987; Helms et al., 2008). Other point observations, such as snow pillows (Coles et al., 1985), acoustic sensors (Kinar and Pomeroy, 2009, 2015b), and passive gamma sensors (Smith et al., 2017), are valuable automated data sources but are spatially limited in extent and can often suffer from location/elevation bias – as demonstrated by the SNOTEL network in the western United States (Molotch and Bales, 2006). In particular, measurements of snow in forest clearings will have relatively more snow than under the adjacent canopy (Pomeroy and Gray, 1995), and so they may not be suitable for snow hydrology calculations or model validations in forested regions even though they are often used for just such purposes. Other techniques need to be developed to capture the small-scale spatial variability of snow–vegetation interactions to advance our process understandings and validate the next generation of distributed snow models.

Remote sensing approaches have shown promise in evaluating snow depth in open areas. Airborne-lidar and UAV structure-from-motion (SfM) approaches have been proven to provide snow depth mapping abilities when differencing snow-covered (hereafter snow) and snow-free (hereafter ground) digital elevation models (DEMs). Lidar, an active sensor, emits a pulse of light, and the detection of the reflected pulse results in a point cloud of a scene with a consistent quality point cloud regardless of flight characteristics,

wind conditions, or solar illumination. A clear benefit of lidar is that multiple returns per pulse can be observed with returns possible from within the canopy and from the sub-canopy ground or snow surface. In contrast UAV SfM uses a passive RGB sensor where data quality is not actively controlled. This results in variable image quality because inconsistent solar illumination influences image exposure, wind gusts influence platform stability leading to blurry images and inconsistent overlap, and surface heterogeneity means that some areas of the domain will have more key points – points automatically detected and matched in multiple images (Westoby et al., 2012) – leading to variability in the quality of the SfM solution (Bühler et al., 2016; Harder et al., 2016; Meyer and Skiles, 2019). So while SfM can provide similar quality error metrics in open areas, the quality will vary between flights as conditions change, whereas lidar will be more consistent. Reported snow depth accuracy in open environments, expressed as root mean square errors (RMSEs), varies from 0.08 to 0.60 m for airborne lidar (Currier et al., 2019; DeBeer and Pomeroy, 2010; Harpold et al., 2014; Mazzotti et al., 2019; Painter et al., 2016; Tinkham et al., 2014), 0.17 to 0.30 m for airborne SfM (Bühler et al., 2015; Meyer and Skiles, 2019; Nolan et al., 2015), and 0.02 to 0.30 m for UAV SfM (Harder et al., 2016; Vander Jagt et al., 2015; De Michele et al., 2016). A notable challenge is that the presence of exposed vegetation, especially dense forest, confounds SfM solutions and obscures airborne-lidar bare-surface extractions which are needed for fine-scale differencing of DEMs to evaluate snow depths or snow depth changes (Bhardwaj et al., 2016; Deems et al., 2013; Harpold et al., 2014). Terrestrial laser scanning (TLS) is another approach for observing high-resolution snow depth data which has been used to develop an understanding of snow depth distributions and for validating other snow depth observation methods (Currier et al., 2019; Egli et al., 2012; Grünwald et al., 2010; Mott et al., 2011). However, TLS has important limitations that restrict further landscape-scale understanding of snow processes in forested areas as it is limited by the site-specific viewshed and viewing geometry (Deems et al., 2013) and occlusion by forest canopies and low vegetation, which decreases point cloud density away from forest edges (Currier et al., 2019). TLS remains an excellent technique for detailed examination of the forest-edge snow environment.

Most applications of remote sensing for observing snow processes have focussed on open environments. However, vegetated portions of those same environments can play a large role in landscape-scale snow hydrology. For example, wetland vegetation accumulates deep snowdrifts and so has an exaggerated influence on snow accumulation processes in prairie environments (Fang and Pomeroy, 2009). Similarly, forests constitute large fractions of the mountain domain (Callaghan et al., 2011; Troendle, 1983) and have very different snow processes than those found in open environments (Pomeroy et al., 2002). Snow–vegetation interactions are complex (Currier and Lundquist, 2018; Gelfan et al.,

2004; Hedstrom and Pomeroy, 1998; Harder et al., 2018; Mazzotti et al., 2019; Musselman et al., 2008; Parviainen and Pomeroy, 2000; Pomeroy et al., 2001; Zheng et al., 2016) and involve both snow interception by the canopy and wind redistribution to forest edges. In dense forests, vegetation leads to the interception and subsequent sublimation of snow, resulting in an overall decrease in accumulation (Hedstrom and Pomeroy, 1998; Parviainen and Pomeroy, 2000; Reba et al., 2012; Swanson et al., 1986). In open environments, such as prairie, tundra, and alpine, wind redistribution of snow leads to a decrease in snow depth in exposed erodible areas and an increase in snow accumulation over aerodynamically rough surfaces or in sheltered areas where wind speeds decrease and snow is deposited – this includes forest edges (Busseau et al., 2017; Essery et al., 1999; Fang and Pomeroy, 2009; Liston and Hiemstra, 2011; Pomeroy et al., 1993; Schmidt, 1982). Much of the understanding of snow–vegetation interactions is based on snow surveys, which are limited in scale and extent. Thus, approaches to systematically and efficiently quantify these dynamics across a drainage basin accounting for topographic and vegetative heterogeneity are needed to further develop and test our process understandings.

## Research questions and objectives

The overall motivation of this work is to understand how snow depth, as well as the processes driving its accumulation and ablation, varies across complex vegetated landscapes. Better tools are needed to measure snow at scales that resolve snow–vegetation interactions, which can involve individual trees and small forest gaps. So the specific objectives in this paper are (1) to evaluate the ability of UAV-lidar versus UAV-SfM techniques for measuring snow depth in open and vegetated areas and (2) to articulate challenges and opportunities for UAVs to map sub-canopy snow depth.

## 2 Data and methods

### 2.1 Sites

Several sites from western Canada, which represent a range of surface conditions and snow climates, were selected to test the ability of UAV lidar and UAV SfM to measure snow depth in open and vegetated areas.

Fortress Mountain Snow Laboratory (hereafter Fortress), in Kananaskis, Alberta (50.833° N, 115.220° W), is a research basin operated by the University of Saskatchewan's Centre for Hydrology in support of mountain hydrology research. The 5 km<sup>2</sup> catchment's elevation ranges from 2000 to 2900 m above sea level (a.s.l.). Field observations for this paper focussed on the Fortress Ridge (Fig. 1a), which spans an open alpine environment, a larch treeline zone near 2200 m a.s.l., and a mixed lodgepole pine and subalpine fir forested slope to the valley bottom at 2000 m a.s.l. (Schirmer and Pomeroy, 2020). Shrubs are primarily willows. The area

was developed as an alpine ski resort in the 1960s but is currently a limited-use ski operation without snowmaking, and some open ski runs remain through some of the slopes of interest. Strong winds result in substantial redistribution of snow by blowing snow in this environment (Aksamit and Pomeroy, 2018)

Two study areas in the Canadian Prairies were examined in this study. Both sites provide examples of cropland with hummocky terrain subject to significant blowing snow redistribution (Fig. 1b, c). Windblown snow from upland areas of short vegetation, wheat and barley stubble, is often transported to lower-elevation wetland depressions where it is effectively trapped by wetland vegetation; shrub vegetation types include willows, dogwoods, tall grasses, and reeds while the trees are primarily poplar and willow. One site was located southeast of Saskatoon, Saskatchewan (51.941° N, 106.379° W), hereafter Clavet, with the other site north of Saskatoon, Saskatchewan (52.694° N, 106.461° W), hereafter Rosthern. The main difference between the prairie sites was that Rosthern received more snowfall and developed a deeper snowpack than Clavet in winter 2019. Where results from both sites are aggregated, they are collectively referred to as prairie hereafter.

### 2.2 Data collection

#### 2.2.1 Lidar system

The UAV-lidar system was comprised of a RIEGL miniVUX-1 UAV lidar sensor, integrated with an Applanix APX-20 inertial measurement unit (IMU) and mounted on a DJI M600 Pro UAV platform (Fig. 2a). The miniVUX-1 UAV utilises a rotating mirror to provide a 360-degree line scan with a measurement rate of 100 KHz and up to five returns per shot with a 15 mm precision. The APX-20 provides positional accuracy of <0.05 m in horizontal and <0.1 m in vertical dimensions with a 200 Hz sampling rate and 0.015 degree and 0.035 degree accuracy in roll/pitch and heading, respectively. The payload, 5 kg, approaches the maximum capacity of the M600 Pro platform, so flight parameters to maximise mapping efficiency were set to 7 m s<sup>-1</sup> ground speed and 100 m flight altitude above the surface with parallel flight lines 80 m apart. The UgCS flight control software (SPH Engineering, 2020) was used to generate terrain following flight paths with respect to these parameters and an underlying SRTM DEM. Flight times were conservatively limited to 15 min. The generated UAV-lidar point clouds have densities of approximately 75 points per square metre (pt m<sup>-2</sup>).

#### 2.2.2 Structure-from-motion systems

Coincident surface mapping with SfM used imagery collected by eBee X or eBee Plus fixed-wing UAV platforms with S.O.D.A. RGB cameras from senseFly (Fig. 2b). The longer flight times, up to 70 min, associated with a

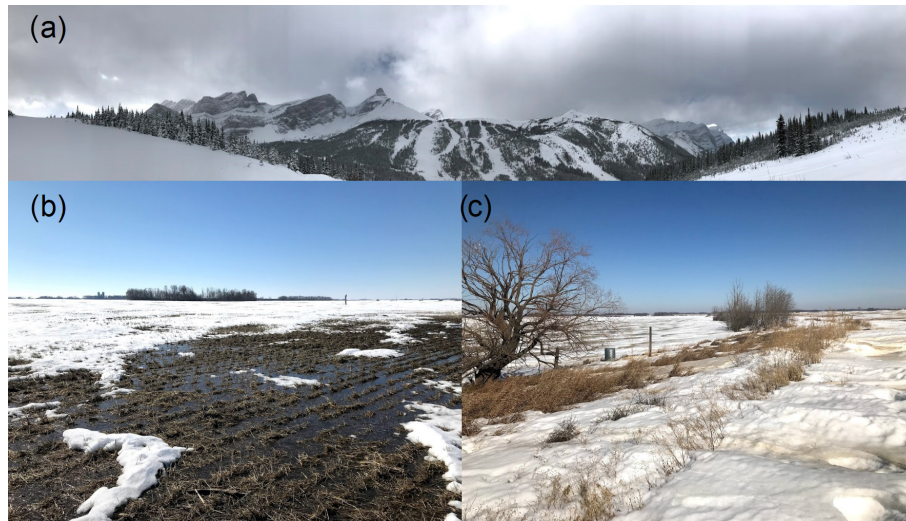


**Figure 1.** (a) Fortress Mountain Snow Observatory in Kananaskis, Alberta, Canada, and (b) Rosthern and (c) Clavet prairie study locations in Saskatchewan, Canada. Data collection was centred on Fortress Ridge (ridgeline in background centre), an area of high topographic variability and a mix of dense forests and clearings. The Rosthern photo highlights the low vertical relief of upland areas and isolated woodlands amongst cultivated fields. The Clavet photo highlights the transition zone between the open upland agricultural terrain and the lower-elevation vegetated wetland.



**Figure 2.** UAV-lidar platform: RIEGL miniVUX-1 UAV mounted on DJI M600 Pro (a). UAV-SfM platform: senseFly eBee X (b).

lightweight payload on a fixed-wing platform allowed for the efficient mapping of large areas. Overlap parameters were generally 80 % for the longitudinal and 65 % for the lateral axes. Flight altitudes of 120 m above the surface provided a ground sample distance of 2.8 cm with the S.O.D.A. camera, which was used on both eBee X and eBee Plus platforms. The generated UAV-SfM point clouds have densities of  $\sim 110 \text{ pt m}^{-2}$ .

### 2.2.3 Ground validation surveys

The assessment of snow depth accuracy used coincident surveys of surface elevation points with Global Navigation

Satellite System (GNSS) surveys and manual measurements of snow depths with a ruler. The intention of the surveys was to validate the spatially distributed snow depth retrievals, and transects were selected in a manner for the surveyor(s) to efficiently sample the greatest variety of vegetation types and gradients. A Leica GS16 base/rover kit provided a real-time kinematic (RTK) survey solution to survey points. The 3D uncertainty of the relative position between the base and rover was computed in real time to be  $< \pm 1.5 \text{ cm}$ , which accounts for errors in signal strength, satellite coverage, and instrument precision. RTK signal quality can degrade in forests, but only points with carrier-phase RTK solutions were used in this analysis, so all survey points are of consistent quality irrespective of vegetation cover. Post-processing of the GNSS data used the Canadian Geodetic Survey of Natural Resources Canada's precise point positioning (PPP) online tool (Natural Resources Canada, 2020) to define an absolute base station location. Due to multi-site logistics, the base station location varied between flights, collection periods ranged between 2.5 and 9 h, and PPP-computed standard deviations were consistently  $< 2 \text{ cm}$ . Post-processing with Leica Infinity software (version 2.4.1.2955) established the absolute positions of the rover points by maintaining the RTK rover base position but adjusting the base station absolute location to that established by the PPP tool. Propagating the uncertainty of the RTK solution ( $\pm 1.5 \text{ cm}$ ) and the PPP-derived absolute base location ( $\pm 2 \text{ cm}$ ) gives an uncertainty of  $\pm 2.5 \text{ cm}$  for the survey points.

**Table 1.** Summary of data collection campaign, September 2018 to April 2019.

Date (mm-dd)	Surface	Data collected	Site	Number of manual observations
09-07	ground	lidar	Rosthern	0
09-19	ground	lidar	Fortress	0
10-10	ground	lidar	Clavet	0
12-13	snow	lidar	Clavet	0
01-31	snow	lidar, SfM	Clavet	51
02-13	snow	lidar, SfM	Fortress	81
03-11	snow	lidar	Clavet	30
03-13	snow	lidar, SfM	Rosthern	111
03-15	snow	lidar	Clavet	35
03-18	snow	lidar, SfM	Rosthern	81
03-20	snow	lidar, SfM	Clavet	69
03-22	snow	lidar, SfM	Rosthern	72
03-24	snow	SfM	Rosthern	0
03-26	snow	lidar, SfM	Rosthern	73
03-29	snow	lidar	Rosthern	77
04-03	snow	lidar	Clavet	0
04-04	snow	lidar	Rosthern	0
04-09	snow	lidar	Rosthern	0
04-25	snow	lidar	Fortress	39

## 2.2.4 Campaigns

To assess the accuracy of the UAV snow depth measurement methods, as well as to provide insight into the seasonally evolving snow depth distribution, a total of 19 flight/manual surveys were conducted at all three study sites between September 2018 and April 2019. These are summarised by date, surveyed surface condition, UAV data collected, and the corresponding number of manually surveyed surface elevation points in Table 1.

## 2.3 Data processing

Snow depth was quantified as the vertical difference between a bare-ground DEM and a bare-snow DEM. This approach was taken regardless of whether the DEMs came from lidar scanning or SfM processing. The workflows implemented to produce DEMs varied between lidar and SfM approaches (Fig. 3), and code is available at <https://github.com/phillip-harder/UAV-snowdepth> (last access: 9 June 2020).

### 2.3.1 Lidar processing workflow

To generate a georeferenced lidar point cloud, several data streams need to be integrated in post-processing. The raw high-frequency trajectory ( $x$ ,  $y$ ,  $z$ , pitch, roll, and yaw) information from the APX-20 IMU was post-processed with POSPac UAV software, which includes a post-processing kinematic (PPK) correction by integrating base GNSS data from a known point <2 km from the flight area, to provide

an absolute sensor position uncertainty of <2.5 cm. The post-processed IMU data are merged with the scanner data within the proprietary RiPROCESS software package to translate the time-of-flight laser returns to an  $x$ ,  $y$ , and  $z$  point. Finally, the alignment of scan lines with overlapping scan data from adjacent flight lines is used to optimise the IMU trajectory with the RiPRECISION tool. This final step in noise reduction improves the final product because the 1.5 cm laser data precision is greater than the post-processed IMU trajectory accuracy.

### 2.3.2 SfM processing workflow

The UAV-SfM processing workflow begins with associating a high-accuracy  $x$ ,  $y$ , and  $z$  position to the images taken. Within the eMotion 3.X software from senseFly, a PPK correction with raw GNSS data collected at the known-point base station is applied to the photo locations to give geotag accuracies of  $< \pm 2.5$  cm. The Pix4Dmapper (v 4.3.33) SfM software, with the “3D Maps” default options template, processed the collected imagery and post-processed geotags to produce a densified point cloud. Within the study sites, a minimum of five ground control points (GCPs), blue 2 m  $\times$  2 m tarps with a white cross, were surveyed with the Leica GS16 rover and integrated into the Pix4D SfM workflow. For further details on how Pix4D implements SfM techniques and, more generally, the approach to use SfM to map snow depth, refer to Harder et al. (2016) and Meyer and Skiles (2019).

### 2.3.3 Point cloud processing

The points representing the “bare” surface, whether that is the snow or ground surface, are of interest for snow mapping. Lidar point clouds comprise returns from vegetation *and* the snow/ground surface, while UAV-SfM point clouds comprise returns from vegetation *or* the snow/ground surface and exhibit substantial noise around snow patch edges (Harder et al., 2016). To remove noise and vegetation points, a noise removal and bare-surface point classification were applied to the point clouds with the LAStools software (Isenburg, 2019). The lidar workflow performed a noise removal followed by a bare-surface point classification. For the bare-ground lidar scans, the height of vegetation (non-ground) points was also calculated. For the SfM workflow, point cloud noise removal and bare-surface classification follow Isenburg (2018).

### 2.3.4 Surface interpolation

A DEM was generated in order to reduce the overall volume of data and to allow for simple surface differencing. The “blast2dem” tool within the LAStools package generates a seamless triangulated irregular network (TIN) that conforms to the point cloud which is then resampled to a raster (Isen-

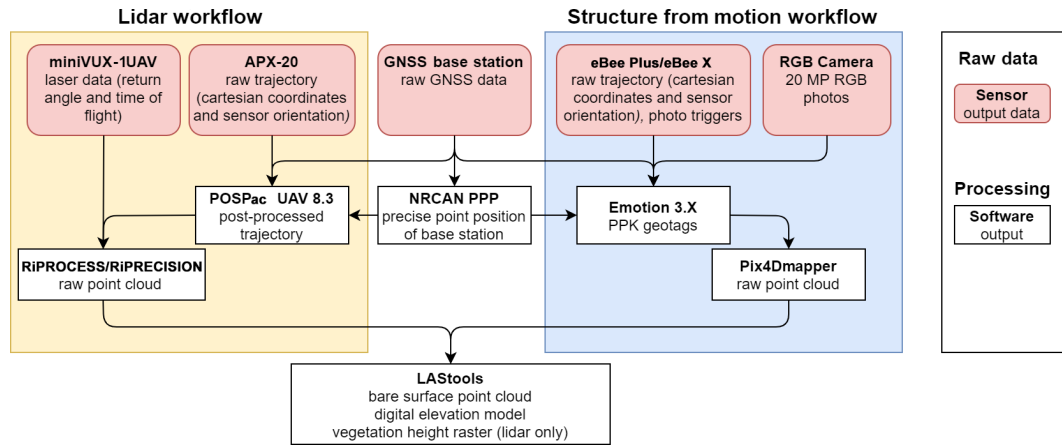


**Figure 3.** Data processing workflows for lidar and SfM point cloud generation.

burg, 2019). A spatial resolution of 0.1 m was applied to all DEMs generated.

### 2.3.5 Error assessment

To assess the accuracy of UAV lidar and UAV SfM with respect to observations, a DEM-based comparison was undertaken. Snow and ground surface values were extracted from the DEM raster cells for locations where a point was manually surveyed and snow depth measured. The snow depth was calculated from the vertical difference between the snow DEM and ground DEM. The influence of vegetation height on snow depth errors was also considered by segmenting the error metrics with respect to vegetation height (open  $<0.5$  m,  $0.5$  m  $\geq$  shrub  $\leq 2$  m, and trees  $>2$  m) derived from the snow-free UAV-lidar scan. The classified vegetation maps and the location of all survey points are visualised in Fig. 4. The error metrics employed to assess the differences between observations and estimates include the root mean square error (RMSE) and the mean bias (mb) (Harder et al., 2016).

### 2.3.6 Point cloud coverage

The continuity of bare-surface point density between UAV-lidar and UAV-SfM methods was quantified in order to interpret how well the respective tools can sense sub-canopy surfaces. All surveys with coincident UAV-lidar and UAV-SfM flights were assessed with the LAStools (Isenburg, 2019) `grid_metrics` function to classify an area with  $>1$  pt per  $0.25$  m<sup>2</sup>, and thereafter they were summarised as percentage areas of each study site with  $>1$  pt per  $0.25$  m<sup>2</sup> with respect to technique. This is a rough metric of DEM quality as it quantifies the relative amount of interpolation needed to translate a point cloud to a continuous surface.

## 3 Results

### 3.1 Accuracy of UAV-lidar versus UAV-SfM snow depth estimates

An accuracy assessment comparing the snow depth from UAV-lidar and UAV-SfM techniques to the manually sampled ground surveys is shown in Fig. 5. UAV lidar has a consistently lower error than UAV SfM in open environments and mountain vegetation. The exception is prairie shrub vegetation where the UAV-lidar RMSE is slightly larger than the UAV-SfM RMSE. The significance of the different relative RMSE values for prairie shrub vegetation is negligible relative to the much larger differences noted in the other domains. UAV-lidar bias is consistently negative ( $-0.03$  to  $-0.13$  m), while the UAV-SfM bias is more variable and both positive and negative ( $0.08$  to  $-0.14$  m).

The influence of vegetation on estimating snow depth from UAVs can be directly assessed by considering the errors associated with different vegetation classes (Fig. 5). When considering UAV lidar, the errors are worse in the presence of vegetation. Open prairie and open Fortress RMSE values are similar (0.09 and 0.1 m RMSE, respectively), while vegetated sites have a larger error (0.13 to 0.17 m RMSE, respectively) with no observed dependency upon vegetation class or type. The sample size of snow depth probe observations is smaller for vegetation sites than open sites, which has implications for error metrics – outliers will have greater weight. The UAV lidar is equally successful at penetrating the open, leaf-off deciduous tree canopy at the prairie sites as the closed, needleleaf canopy at the Fortress site, based on the similar RMSE values within each site's tree vegetation class. The UAV-lidar RMSE for shrub and tree vegetation classes at the Fortress and prairie sites are within 0.04 m. For UAV SfM the errors differ widely for various vegetation covers. The open vegetation has a large RMSE range between

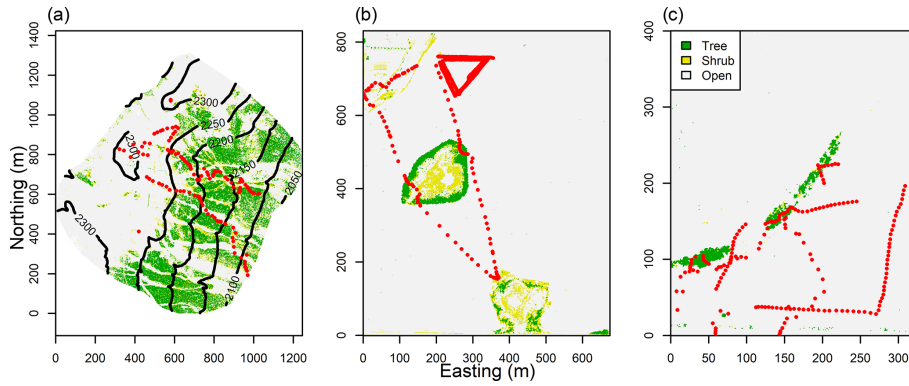


**Figure 4.** Fortress (a), Rosthern (b), and Clavet (c) study sites classified by vegetation height derived from snow-free (ground) UAV lidar into open (<0.5 m), shrub (>0.5 and <2 m), and tree (>2 m) domains. Red points identify locations of manual snow depth survey observations sampled over the course of the data collection campaign. Black lines in the Fortress map are 50 m elevation contours.

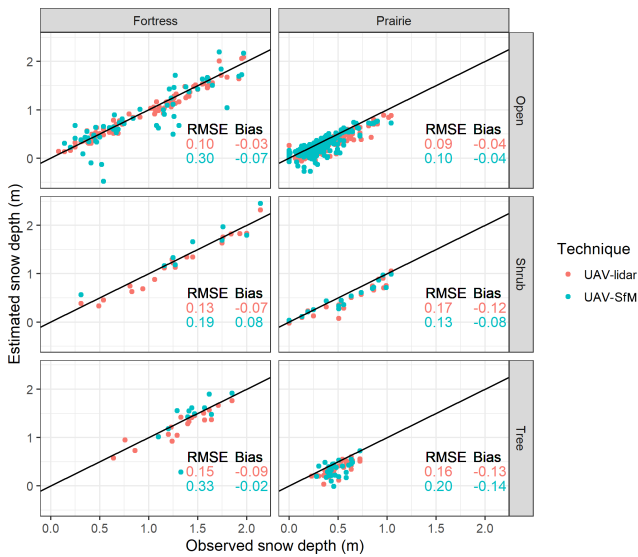


**Figure 5.** Comparison of snow depth observations from snow probes and snow depth estimates from UAV techniques. Plots are segmented within each vegetation class (rows), site (columns), and observation method (colours).

sites (0.1 m in prairie and 0.3 m in Fortress) while vegetation class RMSEs range from 0.13 to 0.33 m.

UAV SfM reports slightly better metrics than UAV lidar in the prairie shrub case: the difference between these techniques is only 0.04 m, which is within the  $\pm 0.025$  m observational uncertainty of the GNSS survey equipment used in this project. The influence of vegetation type is apparent in the UAV-SfM tree class, where the dense needleleaf forest at Fortress has a higher RMSE (0.33 m) than the leaf-off deciduous trees in the prairies (0.2 m). Overall, UAV lidar tends to consistently have lower RMSEs than UAV SfM, which provides confidence in this technique for sub-canopy snow depth mapping.

Snow depth is estimated from differencing the snow and ground DEMs. Therefore, the uncertainty of the snow depth is a propagation of the error of both the snow and ground DEMs. To distinguish which DEM may contribute more to the snow depth error, the remotely sensed surface elevations were compared to the surface elevations from manual GNSS surveys using boxplots (Fig. 6). The boxplots in Fig. 6 illustrate that the UAV-SfM snow-surface elevations have errors consistently greater than the corresponding UAV-lidar surfaces at Fortress. In the prairie snow-surface case, the median RMSE is consistently lower for UAV SfM than UAV lidar, but the UAV SfM does have more variability in its errors. The ground surface was only available from UAV lidar for this study, so no corresponding UAV-SfM ground surface analysis is available. The snow-free UAV-lidar survey has a consistently higher or more variable RMSE than the snow surfaces (with the exception of the open prairie and open and tree Fortress UAV SfM).

### 3.2 Point cloud coverage

The quality of a remotely sensed snow depth estimate is directly tied to how much interpolation is required to fill gaps in a point cloud. The point clouds were classified into areas where  $> 1$  pt per  $0.25 \text{ m}^{-2}$  existed for each technique. Examples of this approach are visualised for the Fortress, Rosthern, and Clavet sites on 14 February and 18 and 20 March 2019 survey dates in Figs. 7–9, respectively. At the Fortress site (Fig. 7b), the large areas of lidar-only points (blue) correspond to areas of forest cover as the UAV-SfM technique could not reliably return surface points with a density  $> 1$  pt per  $0.25 \text{ m}^{-2}$ , while the UAV lidar could. At Fortress, UAV lidar had  $> 1$  pt per  $0.25 \text{ m}^{-2}$  for 93 % of the area of interest versus 54 % for UAV SfM. Considering the black polygons in the Fig. 7a transect, the lack of sub-canopy points identified within the tree vegetation class results in an interpolated snow surface that is erroneously deep under trees, completely missing the detection of the reduced snow depths

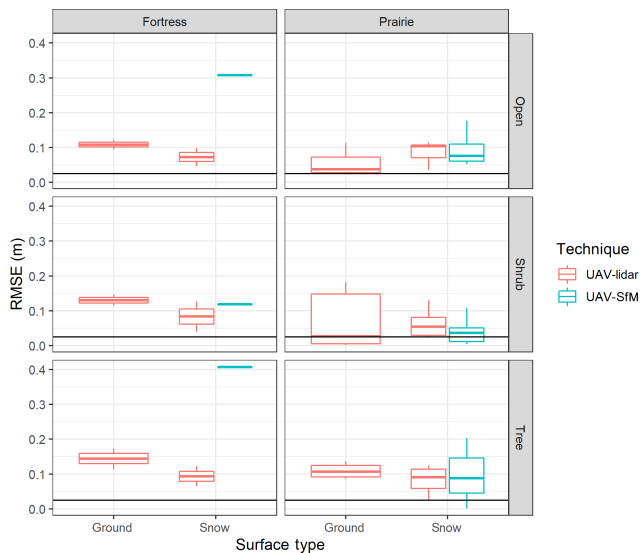


**Figure 6.** Boxplots of RMSEs of UAV-estimated and RTK-surveyed surface elevations segmented by surface condition, technique, site, and vegetation classification. The error metrics approach the  $\pm 2.5$  cm uncertainty of the RTK survey data (black line). Median is indicated by the line within the box: the upper bound is the 75th percentile, the lower bound is the 25th percentile, and whiskers represent the range of values beyond the box.

which are clearly detected (green line) around the base of the trees by UAV lidar. The noisy UAV-SfM points in the middle of the slope (orange polygon) come from vegetation adjacent to the transect. These vegetation points occupied a larger space than the UAV lidar and intruded on the transect line. Therefore vegetation removal from this point in the transect led to a gap in the UAV-SfM point cloud but not the UAV-lidar point cloud. Interpolating through the gap in the UAV-SfM point cloud at this point led to an underestimation of the snow surface. An additional challenge for UAV SfM is open areas with low surface contrast and surface homogeneity, which resulted in large areas without point coverage on the northwest portion of the Fortress study area.

The predominantly open nature of the prairie sites demonstrates a minimal difference in point coverage between the UAV-lidar and UAV-SfM techniques. The average extent of the study domain covered with a point density of  $> 1$  pt per  $0.25 \text{ m}^{-2}$  for five coincident flights at prairie sites was computed, resulting in the mean coverage of 92 % versus 83 % of the study area for UAV lidar and UAV SfM, respectively. As seen in Fig. 8 at the Rosthern site, the areas without UAV-lidar points include some wetland shrubs (green areas in Fig. 8b and c), but predominantly they are randomly distributed points. In contrast, UAV SfM is missing points from areas where the snow surface is very uniform, in vegetated rings around wetlands, and in areas of dense vegetation (blue areas in Fig. 8b and c). These gaps in the UAV-SfM point clouds are interpolated and therefore will represent areas of

greater uncertainty. There was ponded meltwater on the surface of the frozen ground and a frozen wetland water surface at the Clavet site on 20 March 2019, which is responsible for the many areas missing lidar points (green areas) in Fig. 9b. Water is a specular reflector; therefore, unless the lidar has a nadir perspective, water areas will appear as a gap in the point cloud. Fortunately, since water surfaces are flat, minimal interpolation artefacts remain when generating DEMs from the point clouds if the pond edges are sufficiently captured. The challenge in the Canadian Prairies, as seen in the black polygons in Figs. 8a and 9a, is in areas of thick but short vegetation (shrub class) where both lidar pulses and SfM solutions interpret the vegetation surface as the top of the bare ground or snow surface, and therefore little difference exists between DEMs during all measurement periods. An additional challenge of using the UAV-SfM technique is that large gaps in points appear beneath the tall wetland-edge vegetation, leading to points, as visualised in orange polygons in the cross sections of Figs. 8a and 9a, where the estimated UAV-SfM snow surface is below the UAV-lidar ground surface.

## 4 Discussion

### 4.1 UAV lidar is more accurate and consistent than UAV SfM

Snow depth mapping with UAVs has had widespread application in recent years (Bühler et al., 2016; Harder et al., 2016; Vander Jagt et al., 2015; De Michele et al., 2016). The emphasis has been on using SfM techniques to difference DEMs. One of the objectives of this work was to consider the snow depth accuracies possible with the current state of the art of UAV-SfM versus UAV-lidar platforms. What has been demonstrated here is that while there are still errors in UAV lidar (as with any measurement), they are smaller and more consistent relative to UAV SfM. An unavoidable problem for all SfM implementations, which is reflected in this work, is that SfM can only sense the surface – whether that it is the ground/snow surface or the top of a vegetation canopy (Westoby et al., 2012). This makes it fundamentally inappropriate for sub-canopy mapping of snow. Sub-canopy snow depth mapping with UAV SfM therefore becomes an exercise in interpolating snow depth values observed in open areas without vegetation to areas with dense vegetation, rather than sensing the actual snow depth under the canopy. Open areas will have greater snow depths than forest areas (Troendle, 1983; Swanson et al., 1986; Pomeroy et al., 2001; Mazzotti et al., 2019), meaning UAV-SfM solutions, or any approach which requires interpolation of point cloud gaps beneath trees, will overestimate snow (Zheng et al., 2016). The ability of UAV lidar to map snow depths with and without canopy cover and capture tree wells with a  $\text{RMSE} \leq 0.17 \text{ m}$  is an improvement on previous attempts. This RMSE is comparable to previous efforts with UAV SfM (Bühler et al., 2016; De Michele et al.,

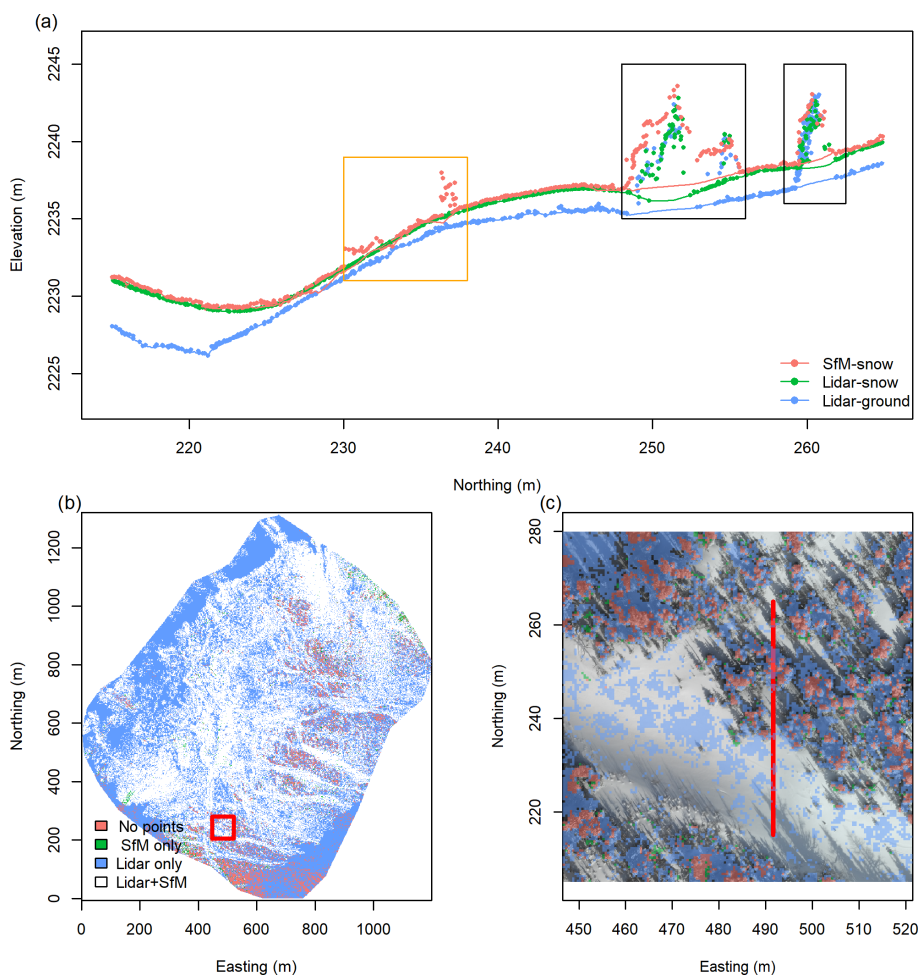


**Figure 7.** Fortress Ridge (14 February 2019) study site with an example (a) cross section with all points and the interpolated vegetation-free surface (lines) for SfM-snow (red), lidar-snow (green), and lidar-ground (blue) surveys. The study area is classified by areas with greater than 1 pt per  $0.25 \text{ m}^{-2}$  in (b) with respect to point clouds obtained from UAV-lidar and UAV-SfM techniques. In (a) black polygons highlight areas of tree wells while the orange polygon highlights an area of UAV-SfM noise on a slope. The red inset polygon in (b) identifies the area of the orthomosaics displayed in (c) with the same overlain transparent point type classification colour scheme as shown in (b). The red line in (c) corresponds to the cross section plotted in (a).

2016; Harder et al., 2016), airborne SfM (Bühler et al., 2015; Nolan et al., 2015; Meyer and Skiles, 2019), and airborne lidar (Deems et al., 2013; Painter et al., 2016), which have been primarily focussed on mapping the snow depth of open snow surfaces. Applications of airborne lidar to forested areas report similar errors (Zheng et al., 2016; Currier et al., 2019; Mazzotti et al., 2019), but the higher flight altitude of airborne platforms and their near-nadir perspective limit point densities near tree centres that are necessary to capture tree wells.

#### 4.2 Bare-surface point cloud coverage is critical

The increased continuous point coverage of UAV lidar is the main advantage over UAV SfM when trying to map sub-canopy snow depth. While snow depth accuracy at times can

be similar between techniques, the ability of UAV lidar to sense a surface below vegetation is critical to develop a coherent snow-surface DEM. The point cloud cross section illustrated in Fig. 7 emphasises these findings, highlighting the wider gaps in the UAV-SfM point cloud beneath individual trees that require interpolation over longer distances, which results in a greater potential for error. Features such as tree wells, where the snow depth decreases with proximity to a tree due to interception/sublimation losses and radiative melting (Pomeroy and Gray, 1995; Musselman and Pomeroy, 2017), will be missed. An interesting dynamic of the RMSEs is that while lidar is comparable across all the sites and vegetation categories, the UAV-SfM RMSE values are much greater in the mountain domain. This is attributed to interpolation artefacts. In prairies where topography is fairly flat, the interpolation of the few gaps can give a reasonable ap-

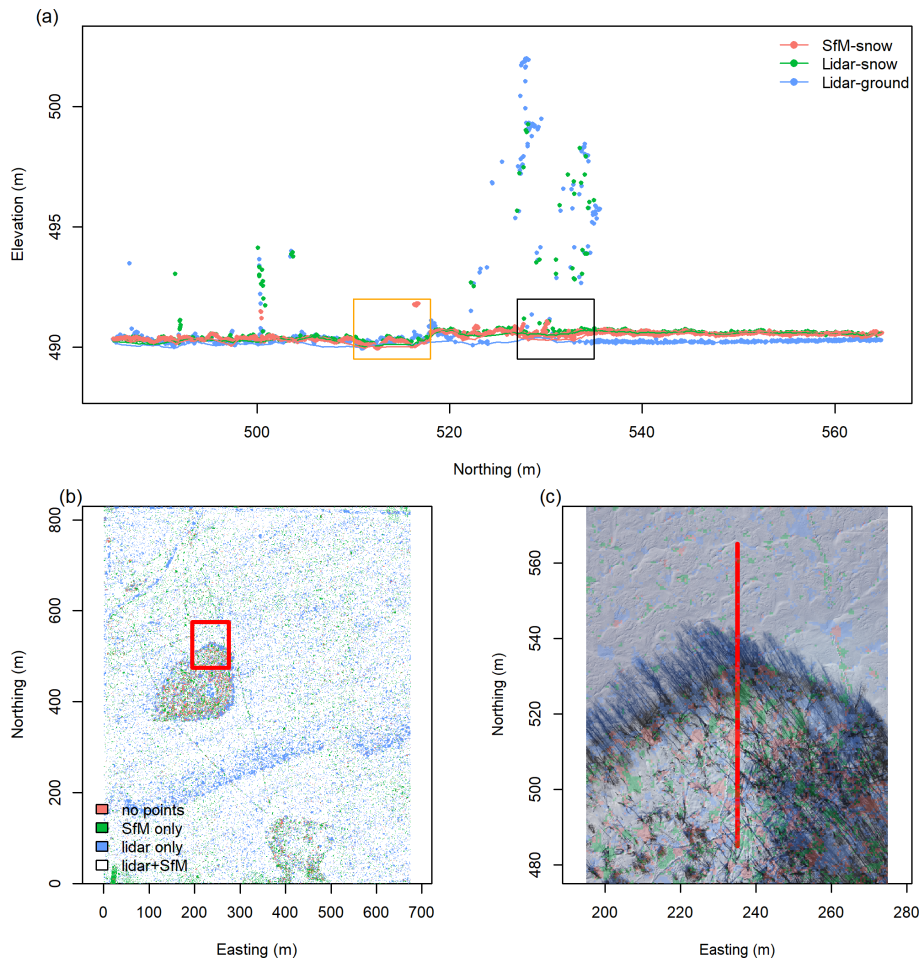


**Figure 8.** Rosthern (18 March 2019) study site with an example (a) cross section with all points and the interpolated vegetation-free surface (lines) for SfM-snow (red), lidar-snow (green), and lidar-ground (blue) surveys. The study area is classified by areas with greater than 1 pt per  $0.25 \text{ m}^{-2}$  in (b) with respect to point clouds obtained from UAV-lidar and UAV-SfM techniques. In (a) the black polygon highlights areas of dense shrubs while the orange polygon highlights interpolation artefacts of UAV SfM. The red inset polygon in (b) identifies the area of the orthomosaics displayed in (c) with the same overlain transparent point type classification colour scheme as shown in (b). The red line in (c) corresponds to the cross section plotted in (a).

proximation of the actual surfaces. In contrast, mountainous regions have a much more complex topography, and the interpolation of large gaps misses much of the small-scale topography and snow–vegetation interaction features. Interpolation works better between two points that are on the same plane (prairies) rather than on a complex non-linear slope (mountains), and where gaps in the point cloud are smaller.

#### 4.3 Lidar snow depth maps and quantifying snow–vegetation interactions

The ability of UAV lidar to map sub-canopy snow depth is established by the consistent error metrics reported, as well as the continuous bare-surface point cloud coverage. The dynamics of snow depth at snow and vegetation process-resolving scales can therefore be examined. Two examples

are presented here to exemplify analyses that are possible with UAV lidar.

##### 4.3.1 Fortress snow depth change

The differences between open and forest snow cover processes can be explored by examining the difference in snow depth between the UAV-lidar scans that took place on 13 February and 25 April 2019 at Fortress. Over this interval, there was intermittent precipitation totaling approximately 100 mm, measured at storage gauges within the study area. The UAV-lidar measured change in snow depth visualises how snow–vegetation interactions translated this snowfall into a snow depth distribution change over a 2 month interval (Fig. 10). In the Fig. 10c cross section, there was accumulation of up to 2 m over the September–April time period on lee slopes, while the upper windswept portions of

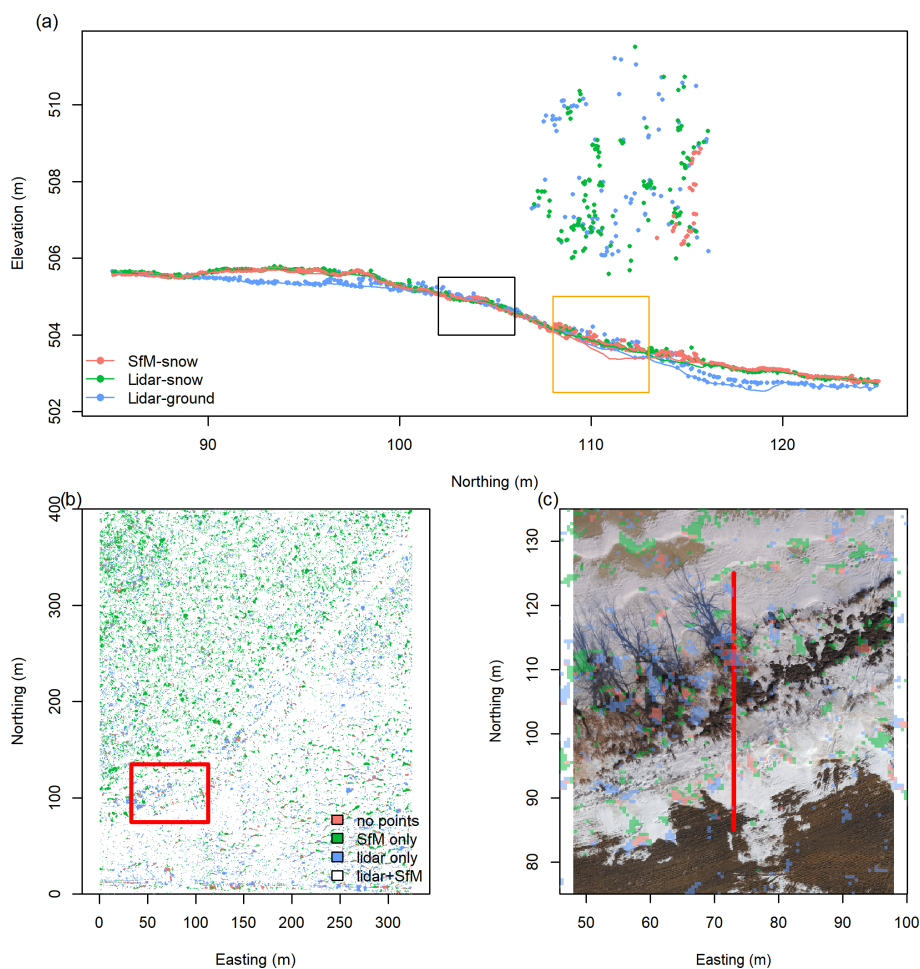


**Figure 9.** Clavet (20 March 2019) study site with an example (a) cross section with all points and the interpolated vegetation-free surface (lines) for SfM-snow (red), lidar-snow (green), and lidar-ground (blue) surveys. The study area is classified by areas with greater than 1 pt per  $0.25 \text{ m}^{-2}$  in (b) with respect to point clouds obtained from UAV-lidar and UAV-SfM techniques. In (a) the black polygon highlights areas of dense shrubs while the orange polygon highlights interpolation artefacts of the UAV SfM. The red inset polygon in (b) identifies the area of the orthomosaics displayed in (c) with the same overlain transparent point type classification colour scheme as shown in (b). The red line in (c) corresponds to the cross section plotted in (a).

the ridge demonstrate snow erosion between February and April. The dynamics and extents of blowing snow sources (grey/red) and sinks (blue) are clearly visualised in Fig. 10a, which closely match the findings of Schirmer and Pomeroy (2020), who used SfM for the same study region. In the forest the UAV lidar observed the increasing snow drifts on the tree line (the krummholz and tree islands – blue areas on top of facing slope in Fig. 10a). Within the forested (Fig. 10b) transect, there is a general decline in snow depth from February to April due to melt on a south facing slope (on the left of the figure) and the development of tree wells in the middle of the transect (orange polygons). The Fig. 10b transect demonstrates the lack of wind redistribution in the forest; snow accumulation is consistently observed to be less than precipitation over the transect due to interception losses, while the Fig. 10c transect on the ridgeline demonstrates significant

wind redistribution, and snow accumulation on the lee slope greatly exceeds the observed precipitation.

#### 4.3.2 Prairie peak snow depth and ablation patterns

In the prairies, wind redistribution is the main driver of snow depth spatial variability. Areas of tall vegetation accumulate wind-blown snow from open upwind sources and are typically associated with the deepest snowpacks. In the winter of 2019, the chronology of snow, temperature, and wind events defined the final snow depth distribution (Fig. 11a). The UAV lidar flown on 13 March captures all of these interactions. Deep snow drifts are found in the roadside ditches (linear features of 1.5 m snow depth on the north and northwest corners Fig. 11a), on the edges of wetland vegetation ( $> 1 \text{ m}$  snow depths on edges of wetlands identified by red polygons in Fig. 11a), and the development of a sastrugi dune complex

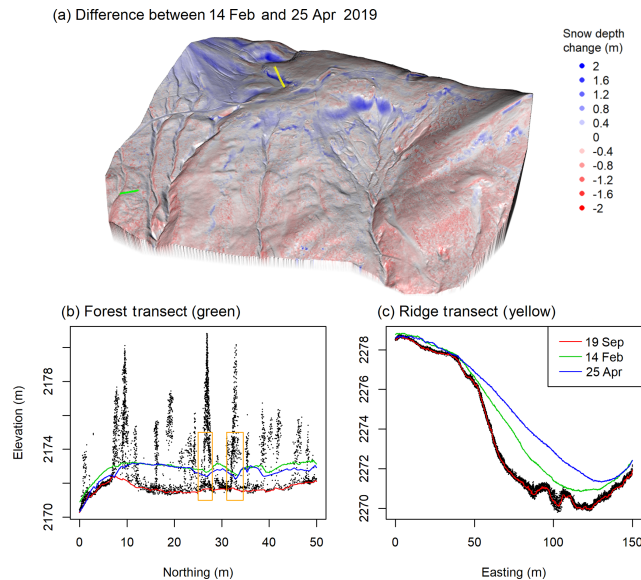


**Figure 10.** (a) UAV-lidar-derived snow depth difference between 13 February and 25 April 2019. Green and yellow lines in (a) correspond to the forest and ridge line transect locations for cross sections in (b) and (c), respectively. Cross-section figures plot the 0.5 m wide point cloud cross section from the 19 September 2018 snow-free scan (black points) to show the point cloud and the processed surfaces of the UAV-lidar scans of the bare ground from 19 September 2018 (red) and the snow surface from 14 February 2019 (green) and 25 April 2019 (blue). Orange polygons in (b) highlight locations of tree wells.

in open areas (parabolic dune shapes and small-scale snow depth variability in middle of Fig. 11a). Areas that the UAV lidar was able to measure correspond to areas where snow depth is the deepest and has important snow–vegetation interactions. In contrast UAV SfM struggles with sensing snow depth on the edges of wetlands as seen by the concentration of lidar-only (blue) areas on the wetland edge in the Rosthern study area (wetland area highlighted by red polygon in Fig. 8b). In the prairies, mapping the areas with deep snow is critical as the deepest snow areas are the ones that dominate runoff generation and runoff contributing areas, are critical for ephemeral wetland ecology, and have the longest snow cover duration with the related runoff timing implications (Fang and Pomeroy, 2009; Pomeroy et al., 2014).

Prairie snowpacks are shallow, leading Harder et al. (2016) to conclude that UAV SfM was unable to capture snow ablation patterns as the signal-to-noise ratio in the open domain was too large, and vegetated area errors were not considered. With the demonstrated ability of UAV lidar to consistently map shallow snow in open areas and deep snow in the vegetated areas, this can be reattempted. Consider the difference in snow depth between 18 and 23 March (Fig. 11b), which represents the earliest part of the active melt period in this particular snowmelt season. Two examples of the spatial variability of process interactions can now be visualised

at the appropriate resolutions. First, the spatial variability of albedo is a major driver of snowmelt. The greatest melt occurs alongside the gravel-covered “grid” roads in the ditches where road dust significantly lowers the albedo, thereby accelerating the melt of the deep snowpacks. Moving eastward from the road ditches into the open fields, there is a decrease in snowmelt depth in the overall scene, visualised in the Fig. 11c transect. This pattern is likely due to the redistribution of dust from the grid roads to the open-field snow surface by the prevailing westerly winds. A snow-surface dust concentration gradient develops over the winter with higher concentrations of dust, and therefore lower albedo (Woo and Dubreuil, 1985), in the west than the east. This increase in albedo, and therefore decrease in solar radiation available to melt snow, corresponds to a decrease in the snowmelt rate (Fig. 11c), moving easterly away from the grid road. Second, the spatial variability of snowpack cold content influences melt rates in the early part of the melt season. Within the agricultural field, the sastrugi drifts are not melting due to the larger cold content of the deep cold snowdrifts relative to the smaller cold content of the shallower surrounding snowpacks. This is also prevalent in the non-melting deep snowdrifts at the vegetated wetland edges. With UAV lidar, a complete picture of the early and asynchronous snowmelt processes is possible. If reliant on UAV SfM, the interpolation needed to fill gaps in the point cloud, near vegetation, and the tops of the sastrugi will obscure the full spatial pattern of snow depth change that conveys the heterogeneity of ablation processes. The high spatial resolution and vertical accuracy of UAV lidar are required to capture these spatial patterns as the length scales of the snow-surface features of interest are small; i.e. sastrugi drifts are on the metre scale, and their changes at daily timesteps are on the centimetre scale.

The processes visualised in the Fortress and Rosthern examples are not new, but the value of UAV lidar is that spatial patterns and changes can be observed across complex landscapes and vegetation gradients with a consistent resolution and accuracy. UAV lidar will therefore be a powerful tool to understand landscape-scale snow–vegetation interactions, as well as to make a core contribution to the validation and improvement of distributed snow process modelling.

#### 4.4 Are the costs and logistics of UAV lidar worth it?

UAV lidar, relative to UAV SfM, provides the ability to measure snow depth below vegetation canopies, but it does come at a higher cost and logistical complexity. There are many similarities between the approaches, and one commonality is that both UAV lidar and UAV SfM require access to a GNSS solution to geolocate point clouds in absolute space. The Leica GS16 package used here is on the expensive side of the spectrum (CAD 70 000), and cheaper equipment, subscription to virtual reference station networks if available in the study area (requires only a rover and not a base station), and

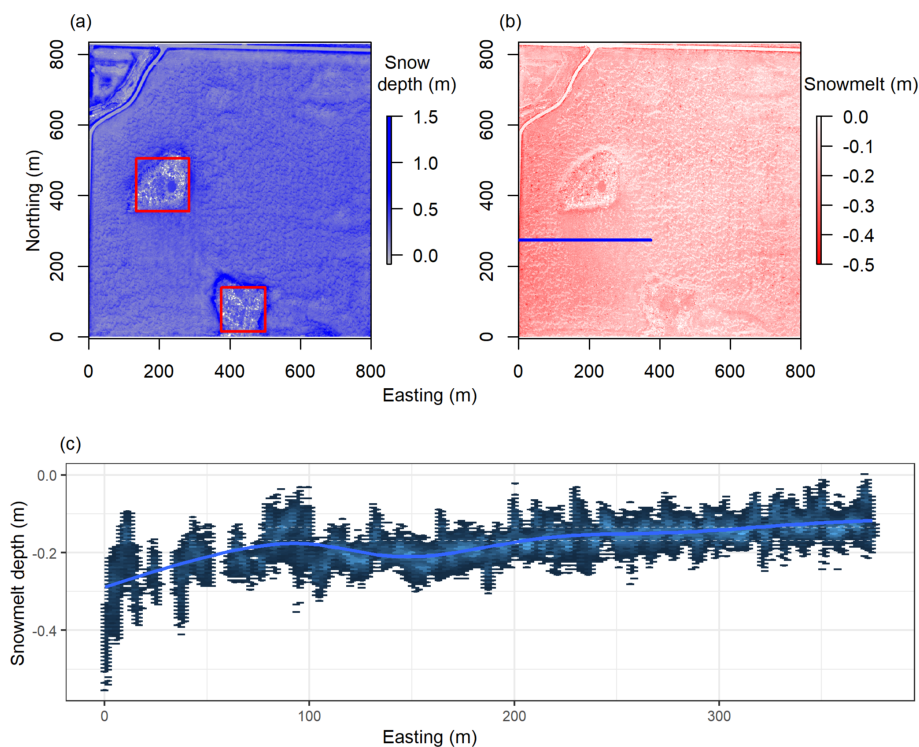


**Figure 11.** Peak snow depth at the Rosthern site from the UAV-lidar scan on 13 March 2019 (a) and snow melt depth difference from the UAV-lidar scans on 18 and 22 March 2019 (b). Snow depth change (c) over a transect (blue line in b) are plotted with a hex plot (to show variability) and smoothed line (to show mean change). Red polygons in (a) highlight wetland areas.

equipment rentals are all viable alternatives to lower costs. The main cost difference between UAV-lidar and UAV-SfM platforms is therefore in terms of the UAV sensor payload. A plethora of UAV-SfM options with and without RTK or PPK photo geotagging are available and can range from small inexpensive systems like consumer grade UAVs (DJI Phantom 3 < CAD 2000) to more expensive options like the senseFly eBee X PPK system (CAD 30 000) used here. Current integrated lidar systems suited to UAV snow mapping (laser wavelengths < 1000 nm, small size, low weight and power requirements, and absolute errors < 5 cm) remain an order of magnitude more expensive than UAV SfM. The cost of the complete UAV-lidar system (lidar, IMU, software suite, and UAV) used here approached CAD 300 000. New and cheaper UAV-lidar sensor options are coming to market all the time, largely driven by the sensing advances coming from the development of autonomous vehicles, but these need testing and still require high-grade IMU/GNSS solutions to allow for absolute geolocation of point clouds. An underappreciated aspect of UAV lidar is that the IMU/GNSS solutions can often be more expensive than lidar sensor itself. The additional cost of UAV lidar to increase sub-canopy snow depth accuracy in dense forest situations in this application can be simplified to a CAD 15 000 per centimetre reduction in RMSE (difference in equipment costs divided by difference in Fortress tree RMSE). Logistical differences between

UAV lidar and UAV SfM are more subtle than the stark cost difference. UAV SfM simply requires a UAV platform and camera in its basic configuration, and therefore small, high-endurance platforms with small batteries can be easily deployed to map large areas. In contrast, most current UAV-lidar configurations need larger platforms that require more cycles of large battery sets to cover similar areas, which represents a logistical challenge in keeping batteries warm and charged in cold and remote areas. Previous UAV-SfM experience (Harder et al., 2017) demonstrated the need to utilise GCPs even with PPK/RTK photo geotagging to minimise the bias error metric. The low bias of UAV-lidar errors, without assimilating GCPs, removes the need to deploy GCPs for UAV-lidar applications, which can be a large time sink. Data processing software suites and workflows are distinct, but ultimately the same level of geomatics expertise is needed to generate useable information. Despite the lower initial purchase costs and longer flight endurance, the errors and artefacts that UAV-SfM techniques introduce in the sub-canopy snow depth measurements, as detailed in Sect. 4.3.1 and 4.3.2, suggest that UAV SfM is not able to directly measure snow depth in densely vegetated environments. If accurate sub-canopy snow depth is required, UAV lidar is the superior option and therefore worth the added logistics and costs.

#### 4.5 Ongoing challenges and future research needs

The ability of UAV lidar to resolve sub-canopy snow depths is not without challenges. Precise classification of surface points from snow and ground scans are needed to resolve the snow depth at the resolutions needed to confidently capture snow–vegetation interactions. Where there are dense shrubs, the last returns will not necessarily be the snow or ground surface, and therefore last-return methods common to airborne applications will not be appropriate. Sub-canopy snow depth mapping requires careful selection of the appropriate point cloud classification and filtering tools and associated parameters to be able to reliably detect the sub-canopy bare surface and achieve the desired quality and precision in a final point cloud. To preserve the small-scale surface variability, point cloud processing will be less efficient as all points need consideration, and the focus on small-scale features will at times lead to erroneous inclusion of points representing large-scale non-surface objects. The algorithm and parameter decisions also have to be adjusted for each flight and site/environment for UAV SfM due to the variable quality and noise of the generated point cloud.

An especially challenging feature in resolving a ground surface is the presence of low and dense vegetation such as shrubs and wetland reeds. This is evident in looking in the centre of the wetland zones (red polygons) of Fig. 11a where there are negative snow depths calculated. In this case, the lidar pulses cannot penetrate the dense vegetation to the underlying ground surface, and the classified bare-ground points have a positive bias. As snow accumulates, the reeds compress and shrubs bend over to the extent that the corresponding snow surface is below the biased bare-ground surface. In the examples presented above, the areas of negative snow are limited to areas where snow depth is relatively shallow in comparison to the deep snow on the wetland edges. This challenge might also be apparent in other regions such as the Arctic tundra, where shrub bending and burial by snow have been extensively documented (Pomeroy et al., 2006; Sturm et al., 2005). While shrubs are much sparser than wetland reeds, their dynamic change in height and potential to positively bias the ground surface extraction will increase uncertainty of snow depth estimation in these hydrologically significant snow accumulation areas. More powerful lasers and higher scan rates may be able to increase point cloud density and penetration to the ground surface, but current sensors with these characteristics may exceed the payload capacities of most UAV platforms. Advances in bare-surface classification/filtering software tools to address the large noise associated with low and dense vegetation are an obvious avenue of improvement. This avenue is inherently limited, as even a perfect bare-surface extraction algorithm will not identify points at the ground surface if pulses cannot penetrate dense vegetation to the ground surface. The time of year chosen for the ground surface scan, ideally right after snowmelt when vegetation is at its lowest and not growing yet, may minimise

errors. Unfortunately, this may not be feasible if the critical wetland areas are inundated as is often the case in the Canadian Prairies in spring.

Mapping sub-canopy snow depth is important, but the ultimate variable of interest is SWE. The challenge is that at snow–vegetation interaction scales there may be significant variability from snow pack densification being driven by different processes across a landscape (Faria et al., 2000). Densification from wind packing is prevalent in open areas versus metamorphic densification due to temperature gradients in sheltered sub-canopy areas (López-Moreno et al., 2013). Current methods of modelling or measuring snow density are not without problems at these small scales. Modelling snow density will impose conceptual understandings of these processes (Raleigh and Small, 2017; Wetlaufer et al., 2016), which may be inappropriate for the small-scale features that need to be represented – these may miss mechanical densification from snow clumps unloading or dripping from the canopy for example. Observational approaches are also a challenge as typical in situ measurements are destructive, limited in extent, and often too limited to develop robust relationships of depth versus density at both the small local and large landscape scales needed (Kinar and Pomeroy, 2015a; Pomeroy and Gray, 1995). Opportunities may be available to pair UAV lidar with other UAV-borne sensors such as passive gamma ray or snow acoustics (Kinar and Pomeroy, 2015b) to non-destructively develop high spatial and temporal resolution estimates of snow density and ultimately the water equivalent.

## 5 Conclusions

Remote sensing techniques to determine snow–vegetation interactions have consistently been challenged by the presence of vegetation. This work directly considers emerging UAV-lidar and UAV-SfM techniques to address this gap in observational capacity. Based upon extensive data collection at a variety of sites and snow conditions with varying snow–vegetation processes, the ability of UAV lidar to measure sub-canopy snow depth is demonstrated. UAV lidar provides snow depth estimates with RMSEs  $<0.1$  m in open areas and  $<0.17$  m in vegetated areas. The UAV-lidar performance consistently exceeded the UAV-SfM performance and was better than previously reported results in the airborne-lidar and UAV-SfM literature. The ability of UAV SfM to measure snow depth in open areas is validated with respect to the growing body of literature and reconfirms that UAV SfM is fundamentally inappropriate to sense sub-canopy surfaces. The clear advantage of UAV lidar is that, as an active sensor, it provides a high point cloud density that is unaffected by surface homogeneity and allows for reliable bare-surface detection. With UAV lidar we can now confidently observe sub-canopy snow depth on the centimetre scales needed to examine snow–vegetation interactions at research

catchment extents (i.e.  $<5 \text{ km}^2$ ). UAV lidar is an emerging tool that will contribute to improving basin-scale snow accumulation estimates, to the validation and parameterisation of distributed snow models, and to enhancing the understanding of the snow–vegetation interaction process over the landscape scale.

*Code and data availability.* The data underlying this analysis and its documentation are available at <https://doi.org/10.20383/101.0193> (Harder et al., 2020) under a Creative Commons CC-BY-4.0 license. The LAsTools workflows and R code used to complete the analysis are available from <https://github.com/phillip-harder/UAV-snowdepth> (<https://doi.org/10.5281/zenodo.3804691>, Harder, 2020) under a GNU General Public License v3.0.

*Author contributions.* PH designed the field campaigns, performed the data collection, and completed/managed the data processing and analysis. PH, JP, and WH prepared and edited the paper.

*Competing interests.* The authors declare that they have no conflict of interest.

*Acknowledgements.* We gratefully acknowledge the field and data processing assistance from Dong Zhao, Alistair Wallace, Greg Galloway, Robin Heavens, Lindsey Langs, Cob Staines, Andre Bertocini, and Bosse Sottmann. The support of Fortress Mountain Ski Resort, the Natural Sciences and Engineering Research Council of Canada, the Canada Research Chairs Program, Canada First Research Excellence Fund, and Western Economic Diversification Canada, a department of the Government of Canada, made this study possible.

*Financial support.* This research has been supported by the Natural Sciences and Engineering Research Council of Canada (Discovery Grants Program – Snow Hydrology), the Canada Research Chairs Program (Canada Research Chair in Water Resources and Climate Change grant), the Canada First Research Excellence Fund (Global Water Futures grant), and the Western Economic Diversification Canada (Smart Water Systems Laboratory grant).

*Review statement.* This paper was edited by Chris Derksen and reviewed by two anonymous referees.

## References

Aksamit, N. and Pomeroy, J. W.: Scale Interactions in Turbulence for Mountain Blowing snow, *J. Hydrometeorol.*, 19, 305–320, <https://doi.org/10.1175/JHM-D-17-0179.1>, 2018.

Bhardwaj, A., Sam, L., Bhardwaj, A., and Martín-Torres, F. J.: LiDAR remote sensing of the cryosphere: Present applications

and future prospects, *Remote Sens. Environ.*, 177, 125–143, <https://doi.org/10.1016/j.rse.2016.02.031>, 2016.

- Bühler, Y., Marty, M., Egli, L., Veitinger, J., Jonas, T., Thee, P., and Ginzler, C.: Snow depth mapping in high-alpine catchments using digital photogrammetry, *The Cryosphere*, 9, 229–243, <https://doi.org/10.5194/tc-9-229-2015>, 2015.
- Bühler, Y., Adams, M. S., Bösch, R., and Stoffel, A.: Mapping snow depth in alpine terrain with unmanned aerial systems (UASs): potential and limitations, *The Cryosphere*, 10, 1075–1088, <https://doi.org/10.5194/tc-10-1075-2016>, 2016.
- Busseau, B.-C., Royer, A., Roy, A., Langlois, A., and Domine, F.: Analysis of snow-vegetation interactions in the low arctic-subarctic transition zone (northeastern Canada), *Phys. Geogr.*, 38, 159–175, <https://doi.org/10.1080/02723646.2017.1283477>, 2017.
- Callaghan, T., Johansson, M., Brown, R. J., Groisman, P., Labba, N., Radionov, V., Bradley, R., Blangy, S., Bulygina, O., Christensen, T. R., Colman, J. E., Essery, R., Forbes, B. C., Forchhammer, M. C., Golubev, V. N., Honrath, R. E., Juday, G. P., Meshcherskaya, A. V., Phoenix, G. K., Pomeroy, J. W., Rautio, A., Robinson, D. A., Schmidt, N. M., Serreze, M. C., Shevchenko, V. P., Shiklomanov, A. I., Shmakin, A., Sturm, M., Woo, M., and Wood, E. F.: Multiple Effects of Changes in Arctic Snow Cover, *Ambio*, 40, 32–45, <https://doi.org/10.1007/s13280-011-0213-x>, 2011.
- Clark, M. P., Hendrikx, J., Slater, A. G., Kavetski, D., Anderson, B., Cullen, N. J., Kerr, T., Örn Hreinnsson, E., and Woods, R.: Representing spatial variability of snow water equivalent in hydrologic and land-surface models: A review, *Water Resour. Res.*, 47, W07539, <https://doi.org/10.1029/2011WR010745>, 2011.
- Coles, G. A., Graham, D. R., and Allison, R. D.: Experience Gained Operating Snow Pillows on a near Real-Time Basis on the Mountainous Areas of Alberta, in *Workshop on Snow Property Measurement*, Lake Louise, AB, 13 pp., 1985.
- Currier, W. R. and Lundquist, J. D.: Snow Depth Variability at the Forest Edge in Multiple Climates in the Western United States, *Water Resour. Res.*, 54, 1–18, <https://doi.org/10.1029/2018WR022553>, 2018.
- Currier, W. R., Pflug, J., Mazzotti, G., Jonas, T., Deems, J. S., Bormann, K. J., Painter, T. H., Hiemstra, C. A., Gelvin, A., Uhlmann, Z., Spaete, L., Glenn, N. F., and Lundquist, J. D.: Comparing aerial lidar observations with terrestrial lidar and snow-probe transects from NASA's 2017 SnowEx campaign, *Water Resour. Res.*, 55, 6285–6294, <https://doi.org/10.1029/2018wr024533>, 2019.
- DeBeer, C. M. and Pomeroy, J. W.: Simulation of the snowmelt runoff contributing area in a small alpine basin, *Hydrol. Earth Syst. Sci.*, 14, 1205–1219, <https://doi.org/10.5194/hess-14-1205-2010>, 2010.
- Deems, J., Fassnacht, S. R., and Elder, K.: Fractal Distribution of Snow Depth from Lidar Data, *J. Hydrometeorol.*, 7, 285–297, 2006.
- Deems, J., Painter, T., and Finnegan, D.: Lidar measurement of snow depth: a review, *J. Glaciol.*, 59, 467–479, <https://doi.org/10.3189/2013JoG12J154>, 2013.
- De Michele, C., Avanzi, F., Passoni, D., Barzaghi, R., Pinto, L., Dosso, P., Ghezzi, A., Gianatti, R., and Della Vedova, G.: Using a fixed-wing UAS to map snow depth distribution: an evaluation at peak accumulation, *The Cryosphere*, 10, 511–522, <https://doi.org/10.5194/tc-10-511-2016>, 2016.

- Egli, L., Jonas, T., Grünewald, T., Schirmer, M., and Burlando, P.: Dynamics of snow ablation in a small Alpine catchment observed by repeated terrestrial laser scans, *Hydrol. Process.*, 26, 1574–1585, <https://doi.org/10.1002/hyp.8244>, 2012.
- Essery, R., Li, L., and Pomeroy, J. W.: A distributed model of blowing snow over complex terrain, *Hydrol. Process.*, 13, 2423–2438, 1999.
- Fang, X. and Pomeroy, J. W.: Modelling blowing snow redistribution to prairie wetlands, *Hydrol. Process.*, 23, 2557–2569, 2009.
- Faria, D., Pomeroy, J. W., and Essery, R. L. H.: Effect of covariance between ablation and snow water equivalent on depletion of snow-covered area in a forest, *Hydrol. Process.*, 14, 2683–2695, 2000.
- Gelfan, A., Pomeroy, J. W., and Kuchment, L. S.: Modeling Forest Cover Influences on Snow Accumulation, Sublimation, and Melt, *J. Hydrometeorol.*, 5, 785–803, 2004.
- Goodison, B. E., Glynn, J. E., Harvey, K. D., and Slater, J. E.: Snow Surveying in Canada: A Perspective, *Can. Water Resour. J.*, 12, 27–42, <https://doi.org/10.4296/cwrj1202027>, 1987.
- Grünewald, T., Schirmer, M., Mott, R., and Lehning, M.: Spatial and temporal variability of snow depth and ablation rates in a small mountain catchment, *The Cryosphere*, 4, 215–225, <https://doi.org/10.5194/tc-4-215-2010>, 2010.
- Harder, P.: UAV Snow Depth Analysis, Zenodo, <https://doi.org/10.5281/zenodo.3804691>, 2020.
- Harder, P., Schirmer, M., Pomeroy, J., and Helgason, W.: Accuracy of snow depth estimation in mountain and prairie environments by an unmanned aerial vehicle, *The Cryosphere*, 10, 2559–2571, <https://doi.org/10.5194/tc-10-2559-2016>, 2016.
- Harder, P., Helgason, W. D., and Pomeroy, J. W.: Modeling the Snowpack Energy Balance during Melt under Exposed Crop Stubble, *J. Hydrometeorol.*, 19, 1191–1214, <https://doi.org/10.1175/jhm-d-18-0039.1>, 2018.
- Harder, P., Pomeroy, J., and Helgason, W.: Unmanned aerial vehicle structure from motion and lidar data for sub-canopy snow depth mapping, Federated Research Data Repository, <https://doi.org/10.20383/101.0193>, 2020.
- Harpold, A., Guo, Q., Molotch, Q., Brooks, P. D., Bales, R., Fernandez-Diaz, J. C., Musselman, K. N., Swetnam, T. L., Kirchner, P. B., Meadows, M. W., Flanagan, J., and Lucas, R.: LiDAR-derived snowpack data sets for mixed conifer forests across the Western United States, *Water Resour. Res.*, 50, 2749–2755, <https://doi.org/10.1002/2013WR013935>, 2014.
- Hedrick, A. R., Marks, D., Havens, S., Robertson, M., Johnson, M., Sandusky, M., Marshall, H.-P., Kormos, P. R., Bormann, K. J., and Painter, T. H.: Direct insertion of NASA Airborne Snow Observatory-derived snow depth time series into the iSnobal energy balance snow model, *Water Resour. Res.*, 54, 8045–8063, <https://doi.org/10.1029/2018WR023190>, 2018.
- Hedstrom, N. R. and Pomeroy, J. W.: Measurements and modelling of snow interception in the boreal forest, *Hydrol. Process.*, 12, 1611–1625, 1998.
- Helms, D., Phillips, S. E., and Reich, P. F.: The History of Snow Survey and Water Supply Forecasting Interviews with U.S. Department of Agriculture Pioneers., United States Department of Agriculture, Natural Resources Conservation Service, 321 pp., 2008.
- Isenburg, M.: Scripting LAStools to Create a Clean DTM from Noisy Photogrammetric Point Cloud, available at: <https://rapidlasso.com/2018/12/27/scripting-lastools-to-create-a-clean-dtm-from-noisy-photogrammetric-point-cloud/> (last access: 29 May 2019), 2018.
- Isenburg, M.: LAStools – efficient tools for LiDAR processing, version 190812, available at: <http://lastools.org> (last access: 10 June 2020), 2019.
- Jonas, T., Marty, C., and Magnusson, J.: Estimating the snow water equivalent from snow depth measurements in the Swiss Alps, *J. Hydrol.*, 378, 161–167, <https://doi.org/10.1016/j.jhydrol.2009.09.021>, 2009.
- Kinar, N. J. and Pomeroy, J. W.: Automated Determination of Snow Water Equivalent by Acoustic Reflectometry, *IEEE T. Geosci. Remote Sens.*, 47, 3161–3167, 2009.
- Kinar, N. J. and Pomeroy, J. W.: Measurement of the physical properties of the snowpack, *Rev. Geophys.*, 53, 481–544, <https://doi.org/10.1002/2015RG000481>, 2015a.
- Kinar, N. J. and Pomeroy, J. W.: SAS2: the system for acoustic sensing of snow, *Hydrol. Process.*, 29, 4032–4050, <https://doi.org/10.1002/hyp.10535>, 2015b.
- King, J., Pomeroy, J. W., Gray, D. M., Fierz, C., Fohn, P. M. B., Harding, R. J., Jordan, R., Martin, E., and Pluss, C.: Snow – atmosphere energy and mass balance, in: *Snow and Climate: Physical Processes, Surface Energy Exchange and Modeling*, edited by: Armstrong, R. and Brun, E., Cambridge University Press, 70–124, 2008.
- Liston, G. E. and Hiemstra, C. A.: Representing Grass- and Shrub-Snow-Atmosphere Interactions in Climate System Models, *J. Clim.*, 24, 2061–2079, <https://doi.org/10.1175/2010JCLI4028.1>, 2011.
- López-Moreno, J. I., Fassnacht, S. R., Heath, J. T., Musselman, K. N., Revuelto, J., Latron, J., Morán-tejeda, E., and Jonas, T.: Small scale spatial variability of snow density and depth over complex alpine terrain: Implications for estimating snow water equivalent, *Adv. Water Resour.*, 55, 40–52, <https://doi.org/10.1016/j.advwatres.2012.08.010>, 2013.
- Mazzotti, G., Currier, W. R., Deems, J. S., Pflug, J. M., Lundquist, J. D., and Jonas, T.: Revisiting Snow Cover Variability and Canopy Structure Within Forest Stands: Insights From Airborne Lidar Data, *Water Resour. Res.*, 55, 6198–6216, 2019.
- Meyer, J. and Skiles, S. M.: Assessing the ability of Structure from Motion to map high resolution snow surface elevations in complex terrain: A case study from Senator Beck Basin, CO, *Water Resour. Res.*, 55, 6596–6605, <https://doi.org/10.1029/2018WR024518>, 2019.
- Molotch, N. P. and Bales, R. C.: SNOTEL representativeness in the Rio Grande headwaters on the basis of physiographics and remotely sensed snow cover persistence, *Hydrol. Process.*, 20, 723–739, <https://doi.org/10.1002/hyp.6128>, 2006.
- Mott, R., Egli, L., Grünewald, T., Dawes, N., Manes, C., Bavay, M., and Lehning, M.: Micrometeorological processes driving snow ablation in an Alpine catchment, *The Cryosphere*, 5, 1083–1098, <https://doi.org/10.5194/tc-5-1083-2011>, 2011.
- Musselman, K. N. and Pomeroy, J. W.: Estimation of Needle-leaf Canopy and Trunk Temperatures and Longwave Contribution to Melting Snow, *J. Hydrometeorol.*, 18, 555–572, <https://doi.org/10.1175/JHM-D-16-0111.1>, 2017.
- Musselman, K. N., Molotch, N. P., and Brooks, P.: Effects of vegetation on snow accumulation and ablation in a mid-

- latitude sub-alpine forest, *Hydrol. Process.*, 22, 2767–2776, <https://doi.org/10.1002/hyp.7050>, 2008.
- Natural Resources Canada: Precise Point Positioning Online Tool, available at: <https://webapp.geod.nrcan.gc.ca/geod/tools-outils/ppp.php?locale=en>, last access: 8 April 2020.
- Nolan, M., Larsen, C., and Sturm, M.: Mapping snow depth from manned aircraft on landscape scales at centimeter resolution using structure-from-motion photogrammetry, *The Cryosphere*, 9, 1445–1463, <https://doi.org/10.5194/tc-9-1445-2015>, 2015.
- Nolin, A. W.: Recent advances in remote sensing of seasonal snow, *J. Glaciol.*, 56, 1141–1150, 2010.
- Painter, T. H., Berisford, D. F., Boardman, J. W., Bormann, K. J., Deems, J. S., Gehrke, F., Hedrick, A., Joyce, M., Laidlaw, R., Marks, D., Mattmann, C., McGurk, B., Ramirez, P., Richardson, M., Skiles, S. M. K., Seidel, F. C., and Winstral, A.: The Airborne Snow Observatory: Fusion of scanning lidar, imaging spectrometer, and physically-based modeling for mapping snow water equivalent and snow albedo, *Remote Sens. Environ.*, 184, 139–152, <https://doi.org/10.1016/j.rse.2016.06.018>, 2016.
- Parviainen, J. and Pomeroy, J. W.: Multiple-scale modelling of forest snow sublimation: initial findings, *Hydrol. Process.*, 14, 2669–2681, 2000.
- Pomeroy, J., Bewley, D., Essery, R., Hedstrom, N., Link, T., Granger, R., Sicart J.-E., Ellis, C., and Janowicz, R.: Shrub tundra snowmelt, *Hydrol. Process.*, 20, 923–941, 2006.
- Pomeroy, J. W. and Gray, D. M.: Snow accumulation, relocation and management, Science Report No. 7, National Hydrology Research Institute, Environment Canada, Saskatoon, SK, 1995.
- Pomeroy, J. W., Gray, D. M., and Landine, P. G.: The Prairie Blowing Snow Model: characteristics, validation, operation, *J. Hydrol.*, 144, 165–192, 1993.
- Pomeroy, J. W., Holler, P., Marsh, P., Walker, D. A., and Williams, M.: Snow vegetation interactions: issues for a new initiative, in *Soil, Vegetation, Atmosphere Transfer Schemes and Large Scale Hydrological Models*, 299–306, IAHS Publ. No. 270, 2001.
- Pomeroy, J. W., Gray, D. M., Hedstrom, N. R., and Janowicz J. R.: Prediction of seasonal snow accumulation in cold climate forests, *Hydrol. Process.*, 16, 3543–3558, 2002.
- Pomeroy, J. W., Shook, K., Fang, X., Dumanski, S., Westbrook, C., and Brown, T.: Improving and Testing the Prairie Hydrological Model at Smith Creek Research Basin, Centre for Hydrology Report: Report No. 14, Centre for Hydrology, University of Saskatchewan, 2014.
- Raleigh, M. S. and Small, E. E.: Snowpack density modeling is the primary source of uncertainty when mapping basin-wide SWE with lidar, *Geophys. Res. Lett.*, 44, 3700–3709, <https://doi.org/10.1002/2016GL071999>, 2017.
- Reba, M., Pomeroy, J. W., Marks, D., and Link, T. E.: Estimating surface sublimation losses from snowpacks in a mountain catchment using eddy covariance and turbulent transfer calculations, *Hydrol. Process.*, 26, 3699–3711, <https://doi.org/10.1002/hyp.8372>, 2012.
- Schirmer, M. and Pomeroy, J. W.: Processes governing snow ablation in alpine terrain – detailed measurements from the Canadian Rockies, *Hydrol. Earth Syst. Sci.*, 24, 143–157, <https://doi.org/10.5194/hess-24-143-2020>, 2020.
- Schmidt, R. A.: Properties of Blowing Snow, *Rev. Geophys. Sp. Phys.*, 20, 39–44, 1982.
- Smith, C. D., Kontu, A., Laffin, R., and Pomeroy, J. W.: An assessment of two automated snow water equivalent instruments during the WMO Solid Precipitation Intercomparison Experiment, *The Cryosphere*, 11, 101–116, <https://doi.org/10.5194/tc-11-101-2017>, 2017.
- Shook, K. and Gray, D. M.: Small-Scale Spatial Structure of Shallow Snowcovers, *Hydrol. Process.*, 10, 1283–1292, 1996.
- SPH Engineering: Universal Ground Control Station (UgCS) Software, Verison 3.4, Latvia, 2020.
- Stappuhn, H. and Dyck, G. E.: Estimating True Basin Snowcover, in *Proceedings of Interdisciplinary Symposium on Advanced Concepts and Techniques in the Study of Snow and Ice Resources*, pp. 314–328, 1974.
- Sturm, M.: White water: Fifty years of snow research in WRR and the outlook for the future, *Water Resour. Res.*, 51, 4948–4965, <https://doi.org/10.1002/2015WR017242>, 2015.
- Sturm, M., Douglas, T., Racine, C., and Liston, G.: Changing snow and shrub conditions affect albedo with global implications, *J. Geophys. Res.*, 110, G01004, <https://doi.org/10.1029/2005JG000013>, 2005.
- Swanson, R. H., Golding, D. L., Rothwell, R. L., and Bernier, P.: Hydrologic effects of clear-cutting at Marmot Creek and Streeter watersheds, Alberta, North. For. Centre, Can. For. Serv. Inf. Rep. NOR-X-278, 33, 1986.
- Tinkham, W. T., Smith, A. M. S., Marshall, H. P., Link, T. E., Falkowski, M. J., and Winstral, A. H.: Quantifying spatial distribution of snow depth errors from LiDAR using Random Forest, *Remote Sens. Environ.*, 141, 105–115, <https://doi.org/10.1016/j.rse.2013.10.021>, 2014.
- Troendle, C. A.: The potential for water yield augmentation from forest management in the Rocky Mountain region, *Water Resour. Bull.*, 19, 359–373, 1983.
- Trujillo, E., Ramirez, J. A., and Elder, K.: Topographic, meteorologic, and canopy controls on the scaling characteristics of the spatial distribution of snow depth fields, *Water Resour. Res.*, 43, W07409, <https://doi.org/10.1029/2006WR005317>, 2007.
- Vander Jagt, B., Lucieer, A., Wallace, L., Turner, M., and Durand, D.: Snow Depth Retrieval with UAS Using Photogrammetric Techniques, *Geosciences*, 5, 264–285, <https://doi.org/10.3390/geosciences5030264>, 2015.
- Westoby, M., Brasington, J., Glasser, N., Hambrey, M., and Reynolds, J.: “Structure-from-Motion” photogrammetry: A low-cost, effective tool for geoscience applications, *Geomorphology*, 179, 300–314, <https://doi.org/10.1016/j.geomorph.2012.08.021>, 2012.
- Wetlaufer, K., Hendrikx, J., and Marshall, L.: Spatial heterogeneity of snow density and its influence on snow water equivalence estimates in a large mountainous basin, *Hydrology*, 3, 3, <https://doi.org/10.3390/hydrology3010003>, 2016.
- Woo, M. and Dubreuil, M. A.: Empirical relationship between dust content and Arctic snow albedo, *Cold Reg. Sci. Technol.*, 10, 125–132, [https://doi.org/10.1016/0165-232X\(85\)90024-2](https://doi.org/10.1016/0165-232X(85)90024-2), 1985.
- Zheng, Z., Kirchner, P. B., and Bales, R. C.: Topographic and vegetation effects on snow accumulation in the southern Sierra Nevada: a statistical summary from lidar data, *The Cryosphere*, 10, 257–269, <https://doi.org/10.5194/tc-10-257-2016>, 2016.